Analysis and modelling of the Optimal Command for a Ultrasound Pulse Inversion Imaging System

Sébastien Ménigot, Jean-Marc Girault

ANALYSIS AND MODELLING OF THE OPTIMAL COMMAND FOR A ULTRASOUND PULSE INVERSION IMAGING SYSTEM

Sébastien Ménigot and Jean-Marc Girault

Université François-Rabelais de Tours, UMR-S930, Tours, France
Inserm U930, Tours, France

2012 European Signal Processing Conference
Bucharest, Romania, 27-31 Aug. 2012
pp 1059 - 1063
ISSN : 2219-5491
Print ISBN: 978-1-4673-1068-0
https://ieeexplore.ieee.org/xpl/login.jsp?tp=&arnumber=6334097
http://www.eurasip.org/Proceedings/Eusipco/Eusipco2012/Conference/papers/1569582641.pdf

ABSTRACT

Over the past twenty years, in ultrasound imaging, contrast and resolution were improved by using the nonlinearties of the medium. One of the most common techniques which used this properties is the pulse inversion imaging. The optimization of this imaging system that we proposed has consisted in finding the optimal command. However, the properties which enable to make an optimal command was not known and that is why we seek the best optimal command by exciting the system by random sequences. In this study, we proposed two steps in our analysis: an analysis and a modelling stage. The proposed model took into account the nonlinearity of the optimal command and enabled to describe the optimal command by using some parameters. If the synthetic model was used in the pulse inversion imaging system, the contrast can reach the same performances.

Index Terms— Modelling, optimal command, optimization, pulse inversion, ultrasound imaging.

1. INTRODUCTION

Over the past twenty years, improvements in sensitivity of ultrasound imaging systems have provided more accuracy of contrast and resolution in medical applications [1] as well as in nondestructive testing [2]. The use of ultrasound imaging was revolutionized when the nonlinear interaction between the ultrasonic wave and the medium was taken into account. However, obtaining an ideal method has been limited. Good separation of the harmonic components requires a limited pulse bandwidth [3], which reduces the axial resolution as in second harmonic imaging [4].

Several imaging methods have been proposed to improve contrast and/or resolution. Some techniques have been only based on post-processings, such as second harmonic imaging [4], subharmonic imaging [5], super harmonic imaging [6] or attenuation correction [7]. Other imaging methods are based on post-processings with encoding which can enable to increase the contrast while ensuring a good axial resolution: the pulse inversion imaging [8], power modulation [9], contrast pulse sequencing [10], pulse subtraction [11] and harmonic chirp imaging [12]. The one of the most commonly used is the pulse inversion imaging, that is reason why this study focused on this system in simulation.

For optimally using the pulse inversion imaging, the transmitted pulse must be correctly chosen. The problem is to find the optimal command $x^{\star}(t)$ of the pulse inversion imaging system which provides the best contrast C:

$$x^{\star}(t) = \arg\max_{x(t)} \left(C\left(x(t)\right)\right), \tag{1}$$

Nowadays, although any method can solve satisfactorily and optimally this problem, several techniques have been shown that it was important to find the optimal command to maximize the contrast. The first solution is an analytic solution developped by Reddy and Szeri [13]. Unfortunately, the problem solution requires (i) inaccessible *a priori* knowledge of the medium and the transducer and (ii) hard solver implementation. The second solution carried on regardless the previous difficulties to transform the shape optimization in a suboptimal parametric optimization, *e.g.* the transmit frequency [14]. Another original solution could be a method based on the Monte-Carlo method whose the main drawback is the large number of tests to reach the optimal command. For example, to find the optimal command which maximized

the contrast, the random process needed more one million tests. However, the random process works without inaccessible *a priori* knowledge to find an optimal solution, that is reason why this study used the solution of this method.

In this paper, we proposed to find the properties of this optimal command in order to build an excitation controlled with a low number of parameters transforming the shape optimization problem into a parametric optimization problem. The first aim of this study was to analyze the optimal command of a pulse inversion imaging system. Secondly, we modelized the optimal command from analysis information to describe a new optimized excitation scheme.

2. OPTIMAL COMMAND ANALYSIS

2.1. Pulse Inversion Imaging System

The analysis was applied to the optimal command of the pulse inversion imaging system for a medical application, *i.e.* ultrasound contrast imaging. In this context, the optimal command maximized the contrast C described by the contrast-to-tissue ratio (*CTR*). It is defined as the ratio of the energy E_b backscattered by the area of the medium perfused by ultrasound contrast agents and the energy E_t backscattered by the area of the non-perfused medium [15].

The simulation model of the pulse inversion imaging system [8] followed the same process as an *in-vivo* setup.

The optimal command $x_1(t)$ and the same signal in opposite phase $x_2(t)$ were generated digitally by Matlab (Mathworks, Natick, MA, USA). The transmitted power was equal to the power of a 400 kPa Gaussian-modulated sinusoidal pulse by adjusting the amplitude of the optimal command. They were filtered by the transfer function of the ultrasound transducer; centred at 3 MHz with a fractional bandwidth of 90% at -3 dB. Note that to take into account imperfections in our simulation, a white noise $\varepsilon(t)$ was added to $x_1(t)$. The signal to noise ratio (SNR) was chosen at 50 dB.

The pulses were then sent in a contrast agent and a tissue model. Firstly, the free simulation program BUBBLESIM [16] was used to calculate the oscillation and scattered echo for a contrast agent microbubble by digitally solving a modified version of the Rayleigh-Plesset equation. The ultrasound contrast agent simulated had properties of encapsulated microbubbles of SonoVue (Bracco Research SpA, Geneva, Switzerland). A 1 nm phospholipid monolayer [17] with a shear modulus of 46 MPa [18] imprisons 2.5 μm ball [19] of sulfur hexafluoride gas (SF_6) [19]. Secondly, the tissue responses were simulated by fat globules with a density of 928 kg/m^3 [20]. The computation of their response was based on the Rayleigh backscattering [21] for a small fat ball of 10 μm; this size was chosen to approximate the small size of fat cells.

The echo $y_1(t)$ of the pulse $x_1(t)$ and the echo $y_2(t)$of the pulse $x_2(t)$ were filtered by the transfer function of the same ultrasound transducer. The sum $z(t)$ of the two echoes $y_1(t)$ and $y_2(t)$ formed a radiofrequency line of the image and extract the even harmonic components. Finally, the *CTR* was measured on the sum $z(t)$.

2.2. Temporal and Frequential Analysis

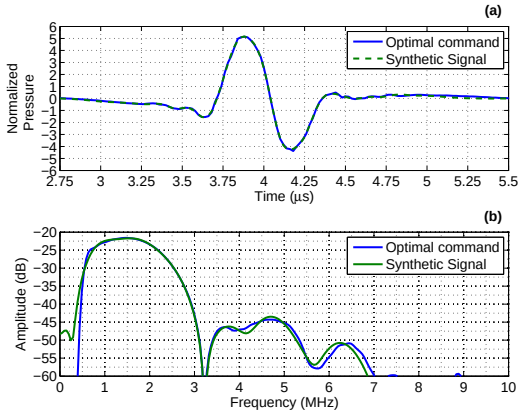

Fig. 1. (a) Optimal command of the pulse inversion imaging and the synthetic signal modelized with orders (8,2) and (b) their respective spectra.

The Fig. 1a shows the optimal command $x_1(t)$ of the pulse inversion imaging system after random optimization process. The optimal command was asymmetric. Firstly, the positive peak was greater than the negative peak. Secondly, the length of the first arch was different to the length of the second arch. The compression was thus more different to the dilatation for the pulse $x_1(t)$ and conversely for $x_2(t)$. Since the nonlinear behavior of the microbubble was sensitive to the phase, the even harmonic components of the microbubble response may be improved as well as the *CTR*. Note that in this case, the *CTR* reached 31.62 dB.

The Fig. 1b shows the spectrum of the optimal command $x_1(t)$. The spectrum revealed harmonic components, in particulary the fourth and the fifth harmonics, whereas the second harmonic was missing. These harmonics components must be responsible to the asymmetry shown in the Fig. 1a.

To summarize our analysis, the optimal command was nonlinear. This result is very important since it is the first time that it has been mentionned. The model of the optimal command must take into account frequential multicomponents by including harmonic components.

3. OPTIMAL COMMAND MODELLING

The aim of the model was to identify the properties of the optimal command by using parameters Ξ. The modelling minimized the mean square error (*MSE*) between the optimal

command $x_1(t)$ and the synthetic signal $\hat{x}(t)$ (Fig. 2):

$$\boldsymbol{\Xi}^{\star} = \arg\min_{\boldsymbol{\Xi}} (MSE) = \arg\min_{\boldsymbol{\Xi}} \left(\sum_{t=0}^{T} \left[x_1(t) - \hat{x}(t) \right]^2 \right) \tag{2}$$

where $\boldsymbol{\Xi}^{\star}$ are the optimal parameters and T the length of the signals. Then the synthetic signal $\hat{x}(t)$ was sent to the pulse inversion imaging in order to verify the good performances of our model in particularly for the *CTR*.

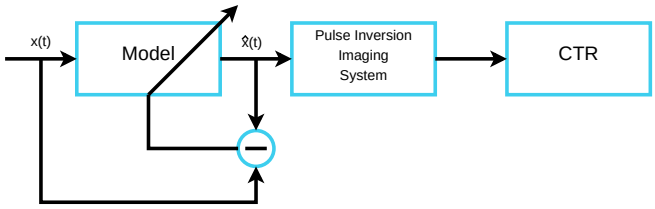

Fig. 2. Block diagram of the optimal command modelling.

From the previous analysis, the optimal command must be modelized by taking into account nonlinearities. The model parameters $\boldsymbol{\Xi}$ must expressed the harmonic components. Moreover, since the contrast agent behavior can have subharmonic components [5], we proposed to add this properties by including half-whole harmonic components. The modelling signal $\hat{x}(t)$ could be written in a base of Gaussian-modulated sinusoidal pulse as follows:

$$\begin{aligned} \hat{x}(t) = G(t) \cdot & \sum_{k=1}^{M} \alpha_{1,k} \cos\left(2\pi k f_0 t + \theta_{1,k}\right) \\ & + \sum_{k=1}^{N} \alpha_{2,k} \cos\left(2\pi \left(k - \frac{1}{2}\right) f_0 t + \theta_{2,k}\right), \end{aligned} \tag{3}$$

where t is the time, $G(t)$ the same Gaussian function used for the random signal, f_0 the optimal frequency, M the number of whole harmonic components, $\alpha_{1,1}, \ldots, \alpha_{1,M}$ the whole harmonic amplitudes, $\theta_{1,1}, \ldots, \theta_{1,M}$ the phases for whole harmonic components, N the number of half-whole harmonic components, $\alpha_{2,1}, \ldots, \alpha_{2,N}$ the half-whole harmonic amplitudes and $\theta_{2,1}, \ldots, \theta_{2,N}$ the phases for half-whole harmonic components. Consequently, the model order was written according M and N such as (M, N). Note that in the case where N is equal to 0, the half-whole harmonic components α_2 and θ_2 were not taken into account.

The modelling required to seek the optimal parameters:

$$\begin{aligned} \boldsymbol{\Xi}^{\star} = [& f_0^{\star}, \alpha_{1,1}^{\star}, \ldots, \alpha_{1,M}^{\star}, \alpha_{2,1}^{\star}, \ldots, \alpha_{2,M}^{\star}, \\ & \theta_{1,1}^{\star}, \ldots, \theta_{1,M}^{\star}, \theta_{2,1}^{\star}, \ldots, \theta_{2,M}^{\star}]. \end{aligned} \tag{4}$$

The optimization frequency was led by an iterative process. Indeed, it was not possible to write the optimization frequency in an algebraic expression unlike for the coefficients α and the phases θ. For each iteration i of the frequency optimization, the coefficients α and the phases θ was optimized by an algebraic process.

3.1. Amplitude and Phase Optimization

This step optimized the amplitudes and the phases for a frequency f_0. In this case, the problem could be written in an algebraic expression by using the trigonometric identity $\cos(a+b) = \cos a \cos b - \sin a \sin b$:

$$\boldsymbol{x} = \boldsymbol{\Psi} \boldsymbol{\vartheta}, \tag{5}$$

where the optimal command was

$$\boldsymbol{x}^T = [x(1), \ldots, x(T)],$$

the amplitudes and phases were collected together such as:

$$\begin{aligned} \boldsymbol{\vartheta}^T = [& \alpha_{1,1} \cos\theta_{1,1}, -\alpha_{1,1} \sin\theta_{1,1}, \ldots, \\ & \alpha_{1,M} \cos\theta_{1,M}, -\alpha_{1,M} \sin\theta_{1,M}, \\ & \alpha_{2,1} \cos\theta_{2,1}, -\alpha_{2,1} \sin\theta_{2,1}, \ldots, \\ & \alpha_{2,N} \cos\theta_{2,N}, -\alpha_{2,N} \sin\theta_{2,N}]. \end{aligned}$$

Finally, the base of Gaussian-modulated sinusoidal pulse were written on a matrix form:

$$\underline{\boldsymbol{\Psi}}^T = \left(\boldsymbol{\Psi}_1, \boldsymbol{\Psi}_2, \ldots, \boldsymbol{\Psi}_T \right),$$

where

$$\begin{aligned} \boldsymbol{\Psi}_t = [& G(t) \cos\left(2\pi f_0 t\right), G(t) \cdot \sin\left(2\pi f_0 t\right), \ldots, \\ & G(t) \cdot \cos\left(2\pi M f_0 t\right), G(t) \cdot \sin\left(2\pi M f_0 t\right), \\ & G(t) \cdot \cos\left(\pi f_0 t\right), G(t) \cdot \sin\left(\pi f_0 t\right), \ldots, \\ & G(t) \cdot \cos\left(2\pi \left(N - 1/2\right) f_0 t\right), \\ & G(t) \cdot \sin\left(2\pi \left(N - 1/2\right) f_0 t\right)] \end{aligned}$$

Finally the coefficients was found by least squares method:

$$\boldsymbol{\vartheta} = (\underline{\boldsymbol{\Psi}}^T \underline{\boldsymbol{\Psi}})^{-1} \underline{\boldsymbol{\Psi}}^T \boldsymbol{x} \tag{6}$$

Note here that a vector is in bold, a matrix was in bold and underlined.

3.2. Frequency Optimization

The frequency optimization was led by an iterative process, because it was not possible to write the problem on an algebraic form. The optimal frequency $f_0^{\star}$ was thus sought by a Newton-Raphson algorithm by minimizing the *MSE* such as:

$$f_{i+1} = f_i - \frac{MSE(f_i)}{MSE'(f_i)}, \tag{7}$$

where i is the iteration and $MSE'(f_i)$ the derivative of the *MSE* when $f_0 = f_i$. However, the analytic *MSE* was not accessible. The algorithm was thus presented in a discrete form [22]:

$$f_{i+1} = f_i - \frac{MSE(f_i)\left(f_i - f_{i-1}\right)}{MSE(f_i) - MSE(f_{i-1})} \tag{8}$$

Note that for each iteration i, there is the amplitude and phase optimization.

3.3. Results

Fig. 3 shows the *MSE* for different orders M and different orders N. For each *MSE*, the parameters $\boldsymbol{\Xi}$ were optimal. The *MSE* decreased when the order M and N increased. The optimal command could be approach by using harmonic and subharmonic components. More precisely, the case without subharmonic imaging (*i.e.* $N = 0$) did not enable to reach the minimum of *MSE*. This result confirmed our hypothesis on subharmonic components.

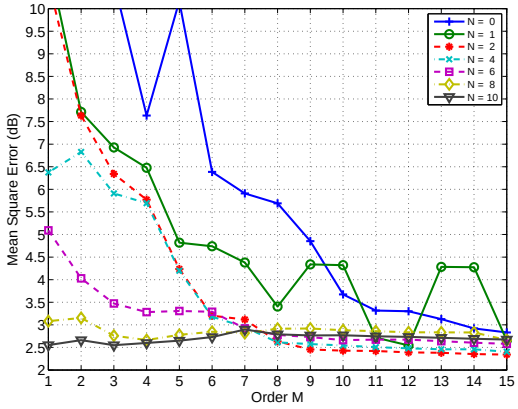

Fig. 3. *MSE* according the order M of whole harmonic components and the order N of half-whole harmonic components.

Fig. 4 shows the *CTR* obtained when the command was modelized with different orders M and different orders N. For each *CTR*, the parameters $\boldsymbol{\Xi}$ were optimal. The *CTR* increased when the order M and N increased. This result confirmed the previous result with the *MSE*. Moreover, when the model used only a linear signal (*i.e.* the model (1,0)), the *CTR* reached 30.3 dB. A linear pulse did not enable to maximize the *CTR* in the pulse inversion imaging system. The best solution was obtained for the model (8,2) where the *CTR* reached 31.58 dB close to the 31.62 dB obtained with the optimal command solved by Monte-Carlo method. As an illustration, the synthetic signal was compared to the optimal command in Fig. 1. The synthetic signal was close and the main error may come with the error of high harmonic components.

Fig. 5 shows the *MSE* during the iterative optimization of the frequency for the model (8,2). To prove the good performances, the empirical *MSE* was measured empirically for the frequency f_0 between 0.5 and 2 MHz. The *MSE* had an only minimum. This result confirmed the use of a local optimization algorithm like the Newton-Raphson algorithm. When the iterative optimization was applied, the *MSE* reached the minimum after around 70 iterations.

Fig. 6 shows the amplitudes α and the phases θ according to the order of the harmonic components for the model (8,2). Note that the optimal frequency was 0.77 MHz. The amplitude coefficients showed that the harmonic components were

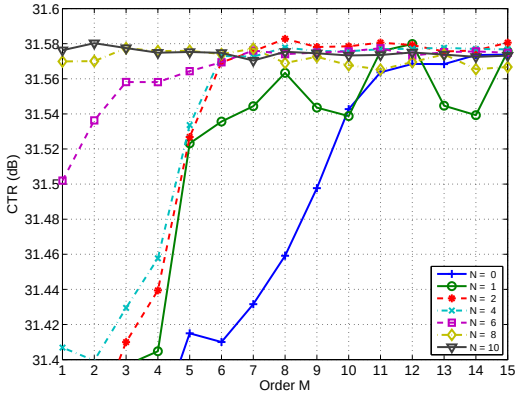

Fig. 4. *CTR* according the order M of whole harmonic components and the order N of half-whole harmonic components when the synthetic signal was sent in the pulse inversion imaging system.

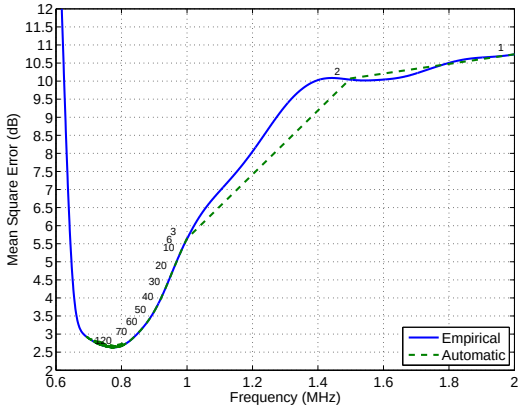

Fig. 5. *MSE* during the iterative optimization of the frequency for the case of the model (8,2).

important and confirmed that the optimal command was nonlinear. Moreover, the phase was different for each component. Indeed, our model was able to take into account the phase of each components unlike in the case of a Volterra model.

4. DISCUSSION AND CONCLUSIONS

Contrast in pulse inversion imaging was optimized by a nonlinear command. The analysis of the optimal command led us to take into account a pulse with many components. More precisely, by using the knowledge of the microbubble behavior, the optimal command was modelized with harmonic and subharmonic components. However, to give more freedom, the resulting model was described by the frequency f_0 of the fundamental, the amplitude and the phase for each components. The advantage of our model was to take into account the phase for each components.

Our model showed us that it was necessary to include har-

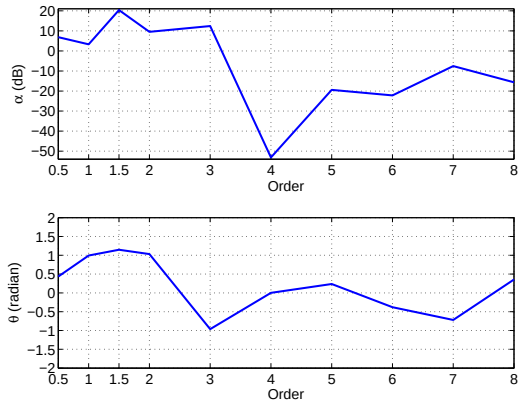

Fig. 6. Amplitudes coefficient α and phase θ for the case of the model (8,2). The optimal frequency was 0.77 MHZ

monic components to reach the best contrast. Usually, a linear input signal was sent to the pulse inversion imaging system without reaching a high contrast. The model was the first step to understand the properties of the optimal command. The modelling signal enabled to reach closer performances of the optimal command.

To conclude, the model described the optimal command with some parameters. This description may help us to seek automatically the optimal command by transforming the shape optimization in a parameter optimization.

5. REFERENCES

[1] P. J. A. Frinking, A. Bouakaz, J. Kirkhorn, F. J. Ten Cate, and N. de Jong, "Ultrasound Contrast Imaging: Current and New Potential Methods," *Ultrasound Med. Biol.*, vol. 26, no. 6, pp. 965–975, July 2000.

[2] J. Blitz and G. Simpson, *Ultrasonic Methods of Non-destructive Testing*, Champman & Hall, London, UK, 1 edition, 1996.

[3] M. A. Averkiou, "Tissue Harmonic Imaging," in *Proc. IEEE Ultrason. Symp.*, 2000, vol. 2, pp. 1563–1572.

[4] P. N. Burns, "Instrumentation for Contrast Echocardiography," *Echocardiography*, vol. 19, no. 3, pp. 241–258, Apr. 2002.

[5] F. Forsberg, W. T. Shi, and B. B. Goldberg, "Subharmonic Imaging of Contrast Agents," *Ultrasonics*, vol. 38, no. 1-8, pp. 93–98, Mar. 2000.

[6] A. Bouakaz, S. Frigstad, F. J. Ten Cate, and N. de Jong, "Super Harmonic Imaging: A New Imaging Technique for Improved Contrast Detection," *Ultrasound Med. Biol.*, vol. 28, no. 1, pp. 59–68, Jan. 2002.

[7] M.-X. Tang, J.-M. Mari, P. N. T. Wells, and R. J. Eckersley, "Attenuation Correction in Ultrasound Contrast Agent Imaging: Elementary Theory and Preliminary Experimental Evaluation," *Ultrasound Med. Biol.*, vol. 34, no. 12, pp. 1998–2008, Dec. 2008.

[8] D. H. Simpson, C. T. Chin, and P. N. Burns, "Pulse Inversion Doppler: A New Method for Detecting Nonlinear Echoes from Microbubble Contrast Agents," *IEEE Trans. Ultrason., Ferroelectr., Freq. Control*, vol. 46, no. 2, pp. 372–382, Mar. 1999.

[9] G. A. Brock-fisher, M. D. Poland, and P. G. Rafter, "Means for Increasing Sensitivity in Non-linear Ultrasound Imaging Systems," *US Patent 5577505*, Nov. 1996.

[10] P. Phillips and E. Gardner, "Contrast-Agent Detection and Quantification," *Eur. Radiol.*, vol. 14, pp. 4–10, Oct. 2004.

[11] J. M. G. Borsboom, A. Bouakaz, and N. de Jong, "Pulse Subtraction Time Delay Imaging Method for Ultrasound Contrast Agent Detection," *IEEE Trans. Ultrason., Ferroelectr., Freq. Control*, vol. 56, no. 6, pp. 1151–1158, June 2009.

[12] J. M. G. Borsboom, C. T. Chin, A. Bouakaz, M. Versluis, and N. de Jong, "Harmonic Chirp Imaging Method for Ultrasound Contrast Agent," *IEEE Trans. Ultrason., Ferroelectr., Freq. Control*, vol. 52, no. 2, pp. 241–249, Feb. 2005.

[13] A. J. Reddy and A. J. Szeri, "Optimal Pulse-Inversion Imaging for Microsphere Contrast Agents," *Ultrasound Med. Biol.*, vol. 28, no. 4, pp. 483–494, Apr. 2002.

[14] S. Ménigot, A. Novell, I. Voicu, A. Bouakaz, and J.-M. Girault, "Transmit Frequency Optimization for Ultrasound Constrast Agent Response," in *IFMBE Proc.*, 2009, vol. 26.

[15] P. Phukpattaranont and E. S. Ebbini, "Post-Beamforming Second-Order Volterra Filter for Pulse-Echo Ultrasonic Imaging," *IEEE Trans. Ultrason., Ferroelectr., Freq. Control*, vol. 50, no. 8, pp. 987–1001, Aug. 2003.

[16] L. Hoff, *Acoustic Characterization of Contrast Agents for Medical Ultrasound Imaging*, chapter 3, pp. 158–160, Kluwer Academic, Boston, USA, 2001.

[17] K. Chetty, C. A. Sennoga, J. V. Hainal, R. J. Eckersley, and E. Stride, "P1F-4 High Speed Optical Observations and Simulation Results of Lipid Based Microbubbles at Low Insonation Pressures," in *Proc. IEEE Ultrason. Symp.*, 2006, pp. 1354–1357.

[18] H. J. Vos, F. Guidi, E. Boni, and P. Tortoli, "Method for Microbubble Characterization Using Primary Radiation Force," *IEEE Trans. Ultrason., Ferroelectr., Freq. Control*, vol. 54, no. 7, pp. 1333–1345, July 2007.

[19] C. Greis, "Technology Overview: SonoVue (Bracco, Milan)," *Eur. Radiol. Suppl.*, vol. 14, no. 8, pp. 11–15, Oct. 2004.

[20] Thomas Szabo, *Diagnostic Ultrasound Imaging: Inside Out*, Academic Press, Oxford, UK, 2004.

[21] J. W. S. Rayleigh, *The Theory of Sound*, vol. 2, chapter 15, pp. 149–154, Macmillan, 1896.

[22] B. Widrow and S. Stearns, *Adaptive Signal Processing*, Prentice Hall, Englewood Cliffs, USA, 1985.